Chemical Engineering Journal 203 (2012) 423–431

Contents lists available at SciVerse ScienceDirect

Chemical Engineering Journal

journal homepage: www.elsevier.com/locate/cej

Adsorption of Pb(II) by iron oxide nanoparticles immobilized *Phanerochaete chrysosporium*: Equilibrium, kinetic, thermodynamic and mechanisms analysis

Piao Xu, Guang Ming Zeng *, Dan Lian Huang *, Cui Lai, Mei Hua Zhao, Zhen Wei, Ning Jie Li, Chao Huang, Geng Xin Xie

College of Environmental Science and Engineering, Hunan University, Changsha 410082, PR China
Key Laboratory of Environmental Biology and Pollution Control (Hunan University), Ministry of Education, Changsha 410082, PR China

HIGHLIGHTS

- MNPs-Ca-alginate immobilized *P. chrysosporium* was explored for Pb(II) removal.
- Pseudo-second-order and Langmuir models best described the Pb(II) adsorption.
- The adsorption was spontaneous and endothermic based on thermodynamic analysis.
- Pb(II) adsorption occurred via the affinity of fungus and the assistance of MNPs.

ARTICLE INFO

Article history:
Received 20 May 2012
Received in revised form 7 July 2012
Accepted 9 July 2012
Available online 20 July 2012

Keywords:
Adsorption
Pb(II)
Phanerochaete chrysosporium
Biomass immobilization
Kinetic
Mechanism

ABSTRACT

A novel adsorbent, iron oxide magnetic nanoparticles and Ca-alginate immobilized *Phanerochaete chrysosporium*, was prepared for removal of Pb(II) ions. Confirmation of the experimental data indicated the pseudo-second-order reaction of the prepared adsorbents. Langmuir isotherm was found to be applicable in terms of relatively high correlation coefficients, which indicated that the adsorption between Pb(II) and the adsorbent was favorable. The thermodynamic analysis showed that the adsorption of Pb(II) was spontaneous and endothermic under the experimental conditions. The adsorption–desorption studies indicated that the prepared adsorbent kept its adsorption efficiencies constant over 5 cycles, maintained about 90%. All the results illustrated that MNPs–Ca-alginate immobilized *P. Chrysosporium* was a very attractive adsorbent for efficient Pb(II) removal from contaminated aqueous solution.

1. Introduction

Heavy metals released into the surface and ground water have been a major preoccupation for many years because of their increased discharge, acute toxicity, non-biodegradable nature and tendency for bioaccumulation [1–3]. Pb(II) is one such heavy metal frequently ran into raw wastewater, as a result of different activities such as industries, mining, and agriculture. Lead is the most representative toxin of the heavy metals which showed toxicological and neurotoxical effects on liver, kidney, brain and central nervous system [4–6]. Problems related with Pb(II) pollution in the environment include irreversible brain damage, nervous disorders, loss of cognitive abilities, severe abdominal pain, dizziness, irritability and weakness of muscles [7–9]. Effective disposal of heavy metal-bearing wastewater is therefore going to be a huge challenge due to the fact that cost-effective treatment alternative is not available.

Increasingly stringent necessity on the wastewater treatment has created a growing interest in the progress of conventional treatment processes [10,11]. During the last few decades, adsorption process combined with magnetic separation has been employed extensively in the processing of wastewater treatment [12]. Field investigations have shown that iron oxide magnetite nanoparticles (MNPs) had gained considerable research attentions in environmental remediation, due to their high surface area and unique superparamagnetism [13]. According to Xu et al. [1], MNPs have also shown considerable potential as immobilization carries, while the utilization of MNPs as support carriers are only sparsely addressed nowadays. First of all, nanoparticles can offer large surface

* Corresponding authors at: College of Environmental Science and Engineering, Hunan University, Changsha 410082, PR China. Tel.: +86 731 88822754; fax: +86 731 88823701.
E-mail addresses: zgming@hnu.edu.cn (G.M. Zeng), huangdanlian@hnu.edu.cn (D.L. Huang).

1385-8947/$ - see front matter © 2012 Published by Elsevier B.V.
http://dx.doi.org/10.1016/j.cej.2012.07.048

areas and more multiple sites for interaction or adsorption [14]. In particular, taking advantage of chemical inertness and favorable biocompatibility, MNPs tends to be an innovative immobilization carrier [15,16]. It is therefore necessary to applied iron oxide MNPs immobilization technology in wastewater treatment.

Generally, immobilization technology could endow adsorbents with mechanical strength, porous characteristics, increased adsorption capacity and moreover stronger resistance to environmental perturbations [17]. Immobilized cells have been attracted great attention since the 1970s [18], mainly profited from the distinct advantages over dispersed cells. Generally, immobilization technology could endow adsorbents with mechanical strength, porous characteristics, increased adsorption capacity and moreover stronger resistance to environmental perturbations [17,19]. It is anticipated that the practical performance will increase significantly after combining with biotechnology and nanotechnology, and large-scale field application will also expand to a great extent. Indeed, there are various as various studies have dealt with heavy metal treatment, but to our knowledge, there is scarce study applied iron oxide magnetic nanoparticles as immobilization carriers for *Phanerochaete chrysosporium* (*P. chrysosporium*).

In our study, we choose *P. Chrysosporium* as biomass strains to optimize the adsorbent, based on the fact that *P. Chrysosporium* is in possession of available capacity to heavy metals [20,21], and MNPs–Ca-alginate immobilized *P. Chrysosporium* was successfully prepared. Batch adsorption experiments were conducted to investigate the adsorption ability of Pb(II) ions from aqueous solution. The adsorption data on kinetic studies were carried out to understand the adsorption process of Pb(II) ions. Experimental equilibrium data at different temperatures were fitted to the Freundlich and Langmuir equations to determine the best fitted isotherm. Besides, thermodynamic study was also performed in this study. Mechanisms of Pb(II) adsorption was primarily explored with the use of FTIR method and intra-particle diffusion analysis. In addition, reusability of the resultant adsorbents was estimated.

2. Materials and methods

2.1. Materials

All reagents used in the experiment were of analytical reagent grade and were purchased from Kermel Tianjin/China. Distilled water was used for the preparation of all the solutions throughout this study. Different concentrations of lead solution were prepared from a stock of 1000 mg/ml solution prepared from analytical grade $Pb(NO_3)_2$. A pH meter (FE20 Mettler Toledo, China) was applied to measure the pH of solutions.

The *P. chrysosporium* (BKMF-1767) was maintained by subculturing on potato dextrose agar (PDA) slants at 4 °C, and then transferred to PDA plates at 37 °C for several days. Spore suspensions were prepared by scraping and blending in the sterile distilled water and then adjusted to a concentration of 2.0×10^6 CFU mL^{-1}.

2.2. Preparation of adsorbents

Iron oxide magnetic nanoparticles (Fe_3O_4 MNPs) and Ca-alginate were encapsulated in the *P. chrysosporium* hyphae pellets. The preparation of adsorbents was conducted by following steps: First, mixed up Na-alginate (40 g L^{-1}, 1 mL) and MNPs (0.10 g), and then sterilization under 115 °C for 30 min. Next, inoculated the mycelium suspensions (2.0×10^6 CFU mL^{-1}, 0.5 mL) into the mixture, and transformed into sterile $CaCl_2$ (0.1 M, 20 mL) solution for dropwise, stewed for 4 h and the *P. chrysosporium* containing microspheres formed. After that, the prepared microspheres were rinsed twice with sterile distilled water and then introduced into 50 mL growth medium as described by Kirk et al. [22]. Finally, the mixture was incubated at 37 °C at 150 rpm. All the above operations were conducted under sterile condition. After 4–5 days of incubation, all samples were harvested for adsorption studies.

2.3. Batch adsorption studies

Adsorption experiments by MNPs–Ca-alginate immobilized *P. chrysosporium* were investigated in a batch equilibrium technique. Adsorbents were mixed with aqueous solution at various Pb(II) initial concentrations in a series of reagent flasks and agitated on a rotary shaker at a constant speed of 150 rpm. All experiments were carried out at pH 5 according to previous study, adjusted by the dilute HCl or NaOH aqueous solution (0.1 M). After adsorption, the supernatant was decanted and the equilibrium concentration of each solution was measured by an atomic absorption spectrometer (AAS, Agilent 3510, USA). All the experiments were carried out in triplicate and data presented were the mean values from these independent experiments. Illustration of the preparation procedure and the whole experiment procedure is presented in Fig. 1.

2.4. FTIR analysis

The Fourier transform infrared spectrophotometer (FTIR) (Nicolet, Nexus-670 FTIR) spectra of the adsorbent were recorded in the range of 4000–400 cm^{-1}, to determine the main functional groups of *P. chrysosporium* available for the binding of Pb(II) for assessment the adsorption mechanism. After 5 days cultivation and adsorption, the adsorbents were collected and rinsed three times, and then freeze-dried for 24 h for the FTIR analysis, through the KBr pressed-disc meth.

2.5. Desorption/reuse studies

The recycling of adsorbent was a most important aspect for an economical process. The regeneration of the adsorbent may be crucially important for keeping the process costs down and opening the possibility of recovering the metals extracted from the liquid phase. For desorption studies, adsorbents were shaken with 50 mL of 0.05 M HCl solution at contact time of 30 min. After desorption, adsorbents were then rinsed twice with distilled water and reintroduced into Pb(II)-containing solutions, at the concentration of 100 mg L^{-1}. The supernatants were collected to determine the Pb(II) concentration by AAS as described above. Meanwhile, this adsorption/desorption cycle was repeated five times to test the reusability of the adsorbents.

2.6. Statistical analysis

The results to be presented were the mean values of three replicates. Standard deviation and error bars were indicated wherever necessary. In all regression cases, the sum of error squared (SSE) between the calculated values and the experimental data can be determined by the following equation:

$$\mathrm{SSE} = \frac{\sqrt{\sum_{i=1}^{N}(q_{\mathrm{exp}} - q_{\mathrm{calc}})^2}}{N}$$

where the subscripts q_{exp} and q_{calc} are the experimental and calculated adsorption capacity, respectively. N is the number of measurements.

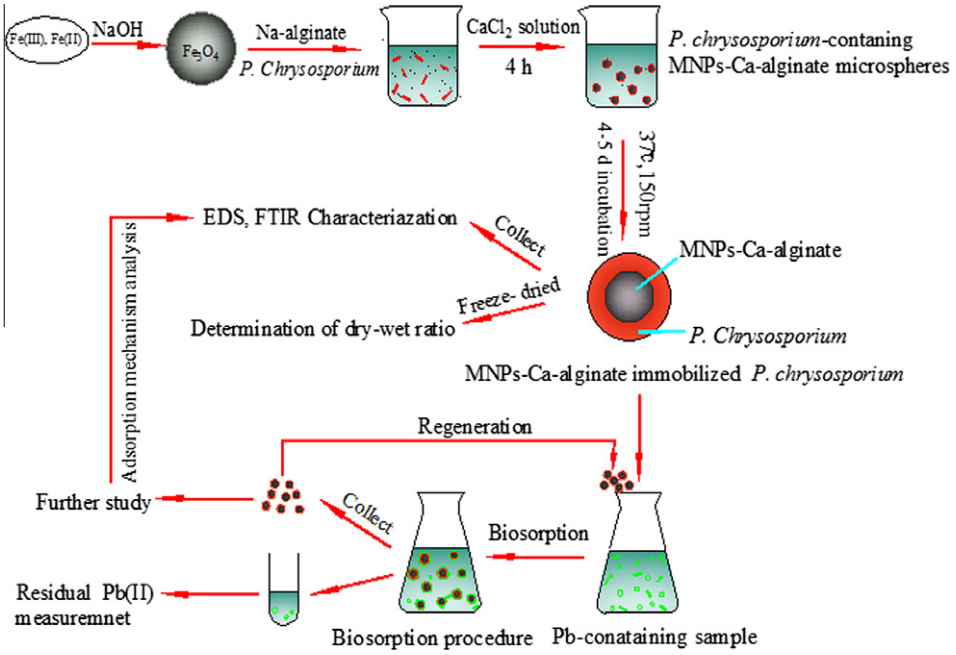

Fig. 1. Schematics of the preparation of MNPs–Ca-alginate immobilized *P. chrysosporium* adsorbents and their application for adsorption of Pb(II).

3. Results and discussions

3.1. Adsorption kinetics

The adsorption rate of Pb(II) on the prepared adsorbents was studied as a function of contact time at pH 5.0 and 35 °C. Residual Pb(II) concentrations in aqueous solution were determined at different times at various initial Pb(II) concentrations of 50, 100, 200 mg L^{-1} and a adsorbent dosage of 1.8 g L^{-1}. Results represented in Fig. 2 described that a rapid adsorption occurred during the first 60 min then followed by a slower adsorption rate. The adsorption equilibrium was achieved within 8 h. These preliminary kinetic experiments strongly suggested that the adsorption of Pb(II) metal ions was a two-step process: a rapid adsorption of metal ions to the surface of bisorbents and followed by possible slow intracellular diffusion in the interior of the adsorbents [23].

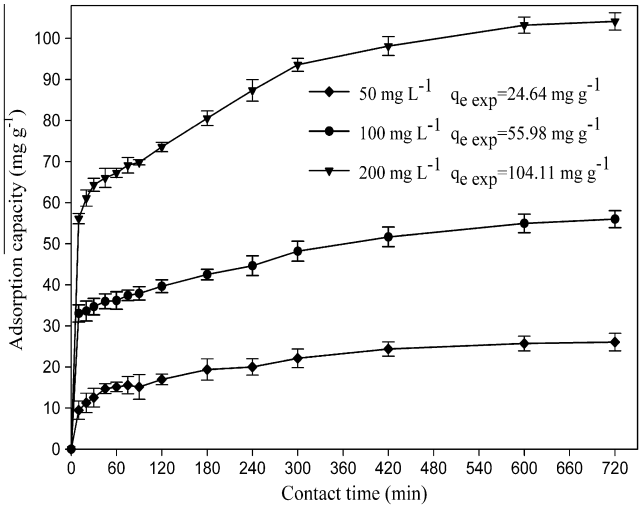

Fig. 2. Effect of contact time on Pb(II) adsorption capacity. pH value: 5.0; temperature: 35 °C; adsorbent dosage: 1.8 g L^{-1}.

Adsorption kinetics studies was evaluated via the capacity of the prepared adsorbent. Adsorption kinetic model, usually applied for estimation of adsorption rate, provides valuable insights into the mechanism of adsorption reactions [24]. Two simple and widely applied models, pseudo-first-order and pseudo-second-order models, were applied to experimental data for kinetic analysis.

3.1.1. Pseudo-first-order kinetics

The linear expression of pseudo-first-order rate based on biosorption capacity is generally described in the following equation [25]:

$$\ln(q_e - q_t) = \ln q_e - k_1 t$$

where q_e and q_t are the amounts (mg g^{-1}) of adsorbed Pb(II) ions on the biomass at equilibrium and at time t, respectively. k_1 is the first-order rate constant (min^{-1}).

The pseudo-first-order kinetic has been established at different initial ions (Fig. 3a). At first 60 min, the rate constant was much higher, and then a pivotal point emerged at 60 min, after that k_1 decreased. The data adequately fitted the pseudo-first order model over the initial course of the experiment (first 60 min), with high correlation coefficients in the range of 0.9970–0.9985 (Table 1).

Theoretically, if the whole process is controlled by a first order mechanism, the values of rate constants (k_1) should be consistent [26]. A two or more linear section of pseudo-first order plot means a multiple pseudo-first order process, each linear section representing a pseudo-first order reaction mechanism. It was obvious that the values of first order rate constants (k_1) varied in our study, a plot of $\ln(q_e - q_t)$ versus time can be divided into two linear sections. Apparently, it indicated a multiple pseudo-first order process. The results were attributed to the heterogeneous nature of the biosorbent surface [27]. In the case of two kinetic steps, the first step of adsorption was more rapid than the second one. According to Varshney et al. [28], in the multiple first order kinetics process, heavy metals were adsorbed on the bound biopolymer at the interface of adsorbents, with negligible interaction between adsorbed Pb(II) ions. While as the adsorption proceeded continuously, the surface monolayer approaches saturation, further increase in the heavy

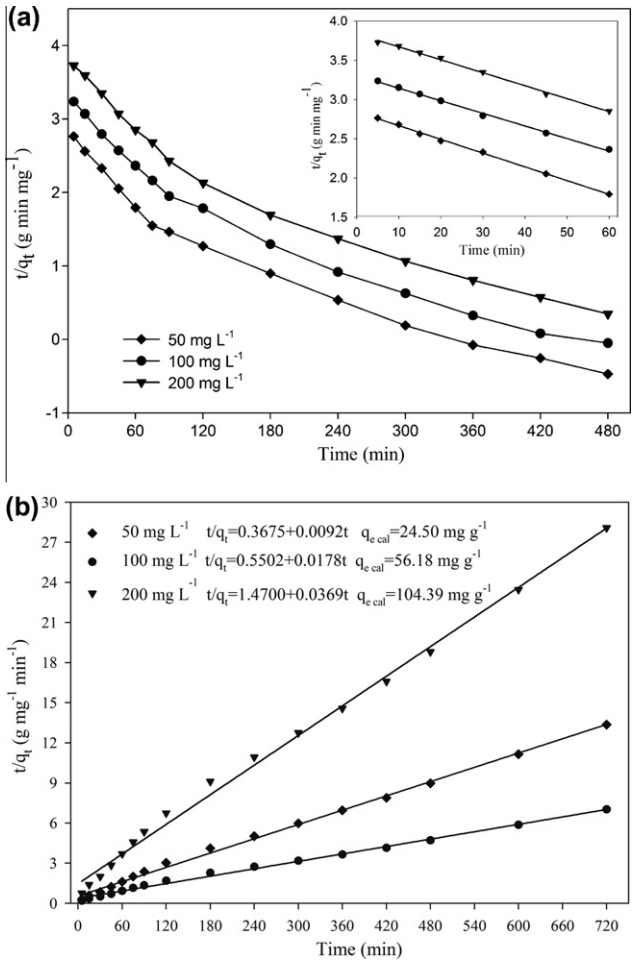

Fig. 3. Linear fit of experimental data for pseudo-first-order (a) and pseudo-second-order kinetic model (b).

metal ions might result in a process of rearrangement, Pb(II) ions may started with intra-particle diffusion [24].

3.1.2. Pseudo-second-order kinetics

The pseudo-second-order equation, based on the assumption that the rate-controlling step, usually correlates the behavior over the whole range of adsorption [24]. The kinetic rate equation is expressed as:

$$\frac{t}{q_t} = \frac{1}{k_2 q_e^2} + \frac{t}{q_e} \quad (1)$$

$$h = k_2 q_e^2 \quad (2)$$

where q_t (mg g^{-1}) is the amount adsorbed at time t, q_e (mg g^{-1}) is the amount of Pb(II) ions adsorbed at equilibrium, k_2 (g mg^{-1} min^{-1}) is the rate constant of pseudo-second-order, h (mg g^{-1} min^{-1}) is the initial sorption rate. The pseudo-second-order kinetic model was applied to describe such adsorption process (Fig. 3b). Fig. 3b showed a plot of the linearized form of the pseudo-second order model, with high values of the correlation coefficients (R^2 = 0.9957–0.9974). This result indicated that this sorption system is a pseudo-second-order reaction, implying that the adsorption mechanism depended on the adsorbate and adsorbent and the rate-limiting step may be a chemical sorption involving valence forces through sharing or exchanging of electrons [24,29].

The values of calculated equilibrium capacities ($q_{e\ cal}$) from the pseudo-second order were almost in accordance with those of experimental capacities ($q_{e\ exp}$) at different initial Pb(II) concentrations (see Table 1). The k_2 values for Pb(II) adsorption were calculated to be 0.917, 0.573 and 0.238 mg mg^{-1} min^{-1} respectively, for 50, 100 and 200 mg L^{-1} Pb(II) adsorption. The low value of rate constant (k_2) suggested that the adsorption rate decreased with the increase in time and the adsorption rate was proportional to the number of unoccupied sites [30]. The initial sorption rate h was 0.68, 1.82 and 2.72 mg g^{-1} min^{-1}, respectively, at the concentration of 50, 100 and 200 mg L^{-1} Pb(II) ions. For any c_0 values within the scope of experiment, the initial adsorption rate h increased with the increase of initial concentrations, indicating that adsorption accelerated with the increment of initial Pb(II) concentration [13,24]. The increase of initial adsorption rate might be because that a kind of driving force was supplied by the higher initial concentration supplied, to overcome the existing mass transfer resistance of Pb(II) ions between the aqueous and solid phases [29].

3.2. Adsorption isotherms

Adsorption isotherms depict the interaction pathway of adsorbates interact with adsorbents [31]. To determine the adsorption model of the adsorbents, isotherms studies were conducted with varying initial Pb(II) concentration from 10 to 500 mg L^{-1}, and analyzed by two adsorption isothermal models: Freundlich and Langmuir isotherm, at different temperatures of 298, 303 and 308 K, as illustrated in Fig. 4. It was obvious from Fig. 4 that temperature of 308 K showed the highest capacity for Pb(II) adsorption by the prepared adsorbents. Maximum adsorption capacity was calculated to be 176.33 mg g^{-1} adsorbent at the initial concentration of 500 mg L^{-1}. Constants and correlation regression coefficients of Pb(II) adsorption are presented in Table 2.

3.2.1. Freundlich isotherm

Freundlich isotherm is an empirical equation based on an exponential distribution of sorption sites and energies, stipulating that the ratio of solute adsorbed to the solute concentration is a function of the solution [30,32]. The Freundlich model is given by the following equation:

$$\ln q_e = \ln K_F + \frac{1}{n} \ln c_e \quad (3)$$

where c_e is the equilibrium concentration of Pb(II) (mg L^{-1}), K_F and n are the Freundlich constants. K_F, which represents the quantity of ions adsorbed onto adsorbent for a unit equilibrium concentration,

Table 1
Kinetics constants for the adsorption of Pb(II) at various concentration.

Pseudo-first order (initial 60 min)				Pseudo-second order				
c_0 (mg L^{-1})	$q_{e\ exp}$ (mg g^{-1})	k_1 (min^{-1})	R^2	$q_{e\ cal}$ (mg g^{-1})	k_2 (mg mg^{-1} min^{-1})	h (mg g^{-1} min^{-1})	R^2	SSE
50	24.64	0.0175	0.9985	24.50	0.917	0.68	0.9957	0.082
100	55.98	0.0165	0.9970	56.18	0.573	1.82	0.9974	0.095
200	104.11	0.0161	0.9973	104.39	0.238	2.72	0.9957	0.091

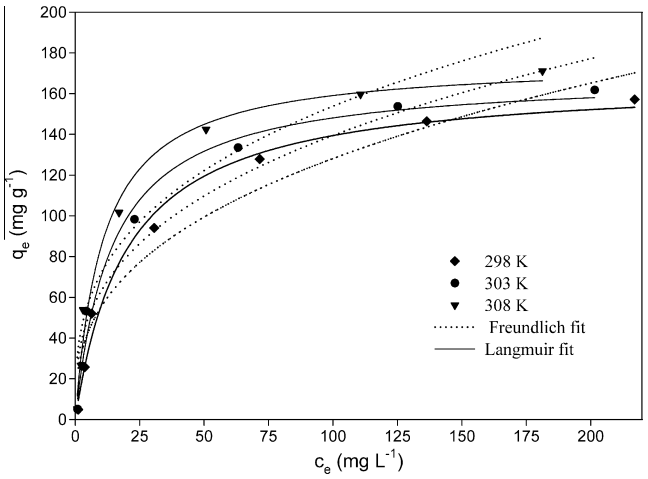

Fig. 4. Adsorption isotherms for Pb(II) onto MNPs–Ca-alginate immobilized *P. chrysosporium* adsorbents at various temperature.

is defined as the adsorption coefficient [30]. The slope $1/n$ was a measure of adsorption intensity or surface heterogeneity. Analysis of Fig. 4 demonstrated that the Freundlich model did not fit the experimental data well. It was observed that K_F varied from 23.72 to 33.36 with the temperature increased from 298 K to 308 K (Table 2), which represented that adsorption quantity has been augmented at higher temperatures, indicating an increased Pb(II)–adsorbent interaction at higher temperature. Generally, $n < 1$ indicated that adsorption intensity was favorable over the whole range of concentrations, while $n > 1$ implied that adsorption intensity was favorable at high concentrations but much less at lower concentrations [26]. In our study, n values were all higher than 1, which indicated that adsorption intensity was good over the whole concentrations ranged from 50 to 200 mg L^{-1}. A value for $1/n$ below one indicates a normal Freundlich isotherm, becoming more heterogeneous as its value gets closer to zero, while $1/n$ above one is an indicative of cooperative adsorption [33]. In our study, the obtained $1/n$ ranged from 0.3663 to 0.3319 (Table 2), which indicated that adsorption process was heterogeneous [34].

3.2.2. Langmuir isotherm

Langmuir isotherm usually has been applied to quantify and contrast the performance of various adsorbents. The Langmuir model, assuming that adsorption takes place at specific homogeneous sites [35], is represented by the following equation [36]:

$$q_e = \frac{K_L q_m c_e}{1 + K_L c_e} \tag{4}$$

$$R_L = \frac{1}{1 + K_L c_0} \tag{5}$$

where q_m is the maximum adsorption capacity (mg g^{-1}), K_L denotes the Langmuir constant (L mg^{-1}) related to the bond energy of the adsorption reaction between metal ion and material, c_0 (mg L^{-1}) is the initial concentration of Pb(II), R_L was the equilibrium parameter or a dimensionless constant separation factor, which could be applied to predict whether the adsorption is favorable. The value of R_L indicated the type of isotherm to be irreversible ($R_L = 0$), favorable ($0 < R_L < 1$), linear ($R_L = 1$) or unfavorable ($R_L > 1$) [37]. Comparing the linear regression values (Table 2), it was concluded that the Langmuir model, capable of representing the data more satisfactorily ($R^2 = 0.9870–0.9895$), yielded a somewhat better fit than the Freundlich model ($R^2 = 0.9330–0.9428$). The adsorption isotherm plots well-fitted Langmuir isotherm, which indicated a reduction of active sites on the adsorbents at a high residual Pb(II) concentration in the solution phase [38]. As depicted in Table 2, at higher temperature, the calculated Langmuir capacity was higher than those at lower temperature, which was consistent with the experimental data. Additionally, with the increase of temperature, stability constant (K_L) for adsorption of Pb(II) got larger, indicating the bond energy between ligand sites of adsorbents and metal ions at higher temperature was larger [31]. The constant (K_L) was the highest for the adsorption at 308 K. Consideringly, the R_L values in this study were calculated in the range from 0.0212 to 0.6676, which indicated the adsorption between Pb(II) and adsorbents was favorable. Moreover, higher R_L was observed at higher temperature, which declared that the adsorption of Pb(II) was more favorable than that at the lower ones. From the slopes and intercepts, the values of q_m were calculated to be 167.36, 169.30 and 176.33 mg g^{-1} at 298 K, 303 K and 308 K, respectively. Table 3 compared maximum adsorption capacities obtained in this study with some other values of white-rot fungi biosorbents and magnetic adsorbents reported in the literature [39–44]. An analytical comparison shows that the prepared adsorbents were better than many other adsorbents in terms of adsorption capacity.

Table 3
A comparison of maximal adsorption capacities (q_m) of white-rot fungi biosorbents and magnetic adsorbents used for Pb(II) removal.

Adsorbents	q_m (mg g^{-1})	Reference
P. chrysosporium	12.34	[44]
Dry *P. chrysosporium*	69.77	[45]
Resting cells of *P. chrysosporium*	80.0	[19]
Loofa sponge immobilized *P. chrysosporium*	134.16	[46]
Fe_3O_4 MNPs	36.0	[47]
m-PAA-Na-coated MNPs	40.0	[13]
PEI-MNPs	83.33	[48]
Magnetic alginate beads	100	[49]
MNPs–Ca-alginate immobilized *P. chrysosporium*	176.33	This study

3.3. Thermodynamic analysis

The temperature of the adsorption medium was of great importance for energy-dependent mechanisms in metal adsorption. Generally, both energy and entropy changes should be considered in any adsorption procedure. The change in free energy ΔG^0, enthalpy ΔH^0 and entropy ΔS^0 associated with the adsorption process were calculated by the following equations [45]:

$$\Delta G^0 = -RT \ln K_L \tag{6}$$

$$\ln K_L = -\frac{\Delta G^0}{RT} = -\frac{\Delta H^0}{RT} + \frac{\Delta S^0}{R} \tag{7}$$

Table 2
Isotherm constants for Pb(II) adsorption onto MNPs–Ca-alginate immobilized *P. chrysosporium* adsorbents at various temperatures.

T (K)	Freundlich model				Langmuir model		
	K_F	$1/n$	R^2	q_m (mg g^{-1})	K_L (L mg^{-1})	R_L	R^2
298	23.72	0.3663	0.9491	167.36	0.0498	0.0386–0.6676	0.9895
303	28.39	0.3456	0.9428	169.30	0.0702	0.0277–0.5875	0.9877
308	33.36	0.3319	0.9330	176.33	0.0924	0.0212–0.5198	0.9870

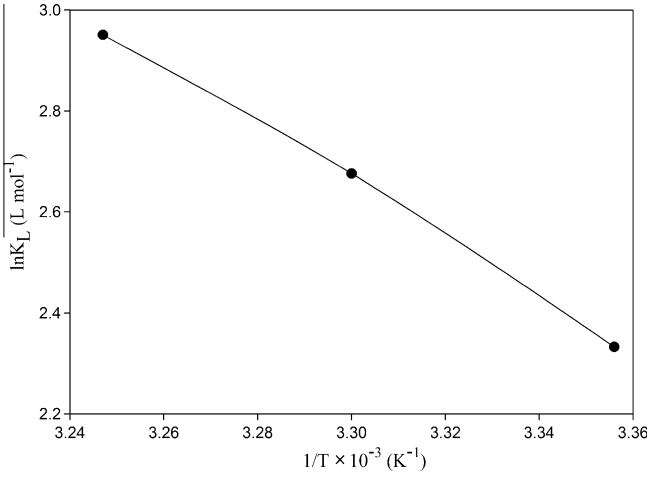

Fig. 5. Plot of $\ln K_L$ versus $1/T$ to predict thermodynamic parameters for the adsorption of Pb(II).

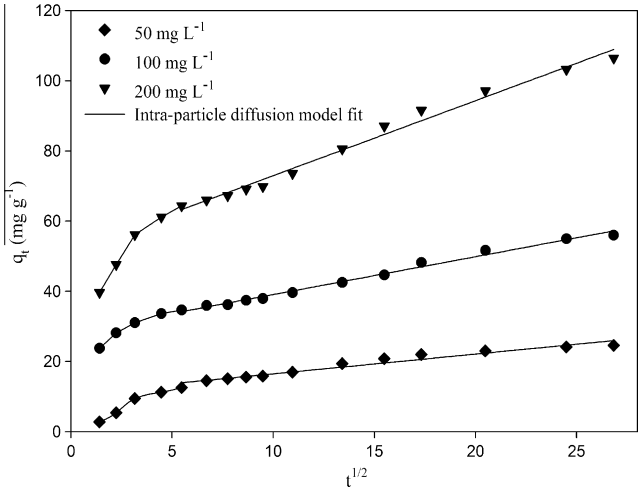

Fig. 6. Linear fit of experimental data for intra-particle diffusion model.

Table 4
Thermodynamic parameters for Pb(II) adsorption on MNPs–Ca-alginate immobilized *P. chrysosporium* adsorbents.

Temperature (K)	ΔG^0 (kJ mol^{-1})	ΔH^0 (kJ mol^{-1})	ΔS^0 (J mol^{-1} K^{-1})	R^2
298	−5.780	47.182	133.47	0.9977
303	−6.374			
308	−7.557			

where R is the gas constant (8.314 J (mol K)$^{-1}$), T is the absolute temperature (K), K_L is the Langmuir constant (L mol^{-1}), ΔH^0 and ΔS^0 could be obtained from the slope and intercept of $\ln K_L$ versus $1/T$ (Fig. 5). Thermodynamic analysis was investigated at three different temperatures (298, 303 and 308 K). The values of the thermodynamic parameters are given in Table 4.

The negative values of ΔG^0 suggested that the adsorption took place spontaneously, and the decreasing of ΔG^0 as temperature rises indicated that the adsorption was more favorable at high temperatures. For an increase in the range of temperature from 298 to 308 K, the adsorption capacity of the prepared adsorbents for Pb(II) showed an increase from 157.20 to 178.19 mg g^{-1}. Moreover, the positive value of ΔH^0 (47.182 kJ mol^{-1}) confirmed the endothermic nature of adsorption and further supported by the increase of adsorption capacity with the increase in temperature. Higher temperature therefore better favored for the adsorption. Furthermore, it may be an indication of ion-exchange adsorption mechanism, which took part with its best Langmuir model fit [46]. While the positive value of ΔS^0 (133.47 J mol^{-1} K^{-1}) may be attributed to the increasing randomness during the adsorption process [35], and further indicated that interactions of Pb(II) with active groups may lead to structural changes of adsorbents [47].

3.4. Adsorption mechanism analysis

3.4.1. Intra-particle diffusion model analysis

The prediction of the rate-limiting step is an important factor to be considered in the adsorption process [32], which is controlled by the adsorption mechanism. According to Paul et al. [48], the adsorption process can be divided into boundary layer diffusion, adsorption of ions onto sites, and intra-particle diffusion. The adsorption of Pb(II) onto the prepared adsorbents may be proceed due to film diffusion firstly and followed by the particle diffusion. Whatever the case, external diffusion will be included in the adsorption process. Intra-particle diffusion model is therefore the most commonly used model for determination the diffusion mechanism involved in the adsorption process [49]. The intra-particle diffusion was determined by the intra-particle diffusion model represented by the following equation [50]:

$$q_t = k_{\text{intra}} t^{1/2} + C$$

where k_{intra} is the intra-particle diffusion rate constant (mg g^{-1} min$^{-1/2}$) and C is a constant related with the thickness of boundary layer (mg g^{-1}).

As shown in Fig. 6, the relationship between q_t and $t^{1/2}$ was considered non-linear over the whole time range, and this indicated that there were several processes proceeding during the adsorption. It could be found that all plots had an initial curved portion, followed by an intermediate linear portion. The figure also verified that adsorption took place in two stages: a very rapid surface adsorption and slow intra-particle diffusion. The initial curved portion was due to boundary layer diffusion or the diffusion of adsorbate through the solution to the external surface of the adsorbents [51]. The followed linear portion of curves was considered to be intra-particle diffusion, which indicated the presence of intra-particle diffusion involved in the process at $t > 30$ min. The values of rate constant for intra-particle diffusion $k_{\text{intra}}/k_{\text{initial}}$ and C/C_0 were listed in Table 5. As presented in Table 5, k_{intra} increased with an increase in the initial Pb(II) concentration. The reason for this result can be attributed to the higher internal diffusion ability in the initial Pb(II) concentration. In the case of the prepared adsorbents, internal transform mechanism has been strengthened in terms of the presence of Ca-alginate and MNPs and consequently avoided the competition for the affinity sites which was common to conventional adsorbents.

The linear plots did not pass through the origin at each concentration, which indicated that intra-particle diffusion may not be the controlling factor in determining the kinetics of the process [52]. In this study, the k_{initial} was 2.4105, 2.5914 and 5.9563, which was far less than $C_0^{1/2}$ (7.07, 10.00 and 14.41). The result further confirmed that intra-particle diffusion was not the only rate-determining step for Pb(II) adsorption, according to the fact that k_{initial} should be close to $C_0^{1/2}$ if the intra-particle diffusion was the only rate-controlling step [53].

3.4.2. FTIR analysis

To data, the principal mechanism of adsorption involves the binding between metal ions and functional groups, and a variety of ligands located on the fungal walls were known to be involved

Table 5
Intra-particle diffusion constants for the adsorption of Pb(II) at various concentration.

C_0 (mg L^{-1})	Stage I (initial 30 min)			Stage II			
	$k_{initial}$ (mg mg^{-1} $min^{-1/2}$)	R^2	$q_{e\ cal}$ (mg g^{-1})	k_{intra} (mg mg^{-1} $min^{-1/2}$)	C (mg g^{-1})	R^2	SSE
50	2.4105	0.9369	24.41	0.5624	10.85	0.9732	0.127
100	2.5914	0.9239	56.32	1.0774	28.31	0.9905	0.093
200	5.9563	0.9419	104.27	2.1362	51.58	0.9870	0.106

in metal chelation (such as carboxyl, carbonyl, amino, amido, sulfonate, sulfydryl, phosphate and so on) on the surface or inside the porous structure of the adsorbents [54,55]. According to Huang et al. [56], the biosorption *P. chrysosporium* ability to Pb ions was might be attributed to the following reasons: (i) Pb ions were chelated by the functional group at the surface of cell walls, accompanied with ion exchange, or (ii) Pb ions were adsorbed on cell walls, due to the abundant polysaccharides, peptides, and pigments existing on cell walls.

To determine the main functional groups of adsorbents in Pb(II) ions adsorption for sorption mechanism assessment, FTIR spectra was employed to analyze the spectra vibration before and after Pb(II) ions loaded (Table 6). It was well known that the electrostatic interactions were too weak to vary the band of the functional groups on the surface [25,57]. Therefore the band shifts suggested that a chelation process took place between functional groups and Pb(II) ions. It can be seen from Table 5 that the obviously shift took place in the bands assigned to C═O at 1645 cm^{-1}, 1417 cm^{-1} and 1257 cm^{-1}, reflected complexation of carboxylate anions functional group by coordination with Pb(II). The most remarkable differences between two spectra was at intensity of 3394 cm^{-1} representing O—H groups and 1325 cm^{-1}, representing N—H groups. The decrease indicated the major role of hydroxyl (—OH) and amide functional groups on the Pb(II) interaction. A slight red-shift happened in the Pb(II)-loaded spectrum at 1076 cm^{-1}, relating to the stretching vibration of P—OH. Importantly, a high band height of Fe—O functional groups has been observed in the FT-IR spectra, in case of the shifts of Fe—O bonds from 627, 588 cm^{-1} to 625, 586 cm^{-1}. This may also be acceptable evidence that Pb(II) was not only attached on the surface of *P. chrysosporium*, but also may form chemical bonds with Fe—O groups of MNPs. It has been confirmed that there were Fe—O functional groups available which signify the major involvement of MNPs for binding of Pb(II).

As stated before, heavy metals were firstly adsorbed on the bound biopolymer at the interface of adsorbents, while as the surface monolayer approaches saturation, a further increase in Pb(II) ions might result in a process of intra-particle diffusion. It meant that metal ions adsorbed on the surface of the adsorbents would transmit to the interior of adsorbents with the saturation of surface binding sites. Especially in the presence of the MNPs and Ca-alginate, the intracellular mechanism was enhanced to a large extent. On one hand, the heavy metals adsorbed to the surface might transmit to the interior of the adsorbents due to the electrostatic attraction between MNPs and heavy metal ions [58], which resulted in the enhancement of adsorption capacity of adsorbents. On the other hand, the structure of embedded MNPs and Ca-alginate was close to a micro-porous 'honeycomb', the resistance to internal diffusion has been diminished. In conclusion, the obtained results were available to demonstrate that both the functional groups of *P. chrysosporium* and the embedded iron oxide nanoparticles played part in the adsorption process.

Table 6
FTIR spectra variation of MNPs–Ca-alginate immobilized *P. chrysosporium* before and after adsorption in the region between 400 and 4000 cm^{-1}.

Adsorbents (cm^{-1})	Pb(II)-loaded adsorbents (cm^{-1})	Functional groups
3394, 1325	3388, 1311	O—H; N—H groups
1645, 1417	1644, 1415	C═O stretching
1257	1250	Amide group
1076	1078	P—OH stretching
1039	1038	C—OH stretching
627, 588	625, 586	Fe—O stretching

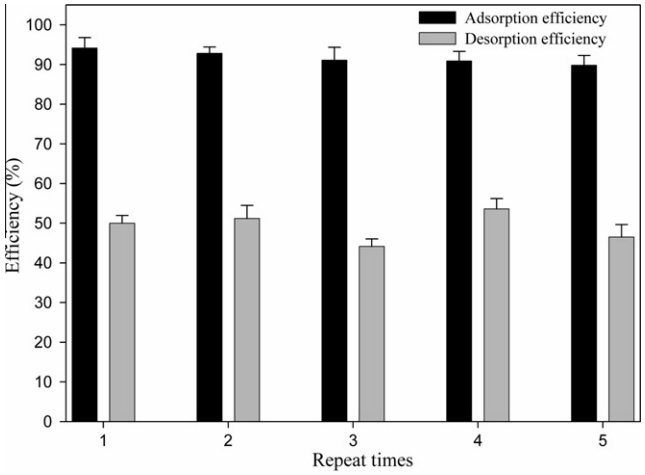

Fig. 7. Five consecutive adsorption–desorption cycles of MNPs–Ca-alginate immobilized *P. chrysosporium* for Pb(II).

3.5. Desorption and reusability

In order to show the reusability of the adsorbents, adsorption–desorption cycles of Pb(II) were repeated five times by reusing the test adsorbents. It can be seen from Fig. 7 that the adsorption efficiency kept constantly, maintaining at about 90% and no obvious difference was observed during five adsorption–desorption cycles. The results showed that the adsorbents were stable with good reusability and could be used repeatedly for the removal of heavy metal ions from wastewater. Such a property was an economic necessity to apply this kind of adsorbent in wastewater treatment.

4. Conclusions

In this work, MNPs–Ca-alginate immobilized *P. chrysosporium* adsorbents were successfully prepared. Equilibrium adsorption data were well fitted by pseudo-second-order kinetic models, which showed higher correlation coefficients. The adsorption process was described well by the Langmuir model, in comparison to the Freundlich model. According to the thermodynamic studies, it was determined that the adsorption process took place spontaneously with a negative free energy. A positive value of standard enthalpy change showed the endothermic nature of adsorption process. Intra-particle diffusion model fitting verified that adsorption took place in two stages: a very rapid surface adsorption and slow intra-particle diffusion. Discussions on the adsorption mechanisms with respect to the FTIR analysis inferred that the

adsorption might be attributed to two possible mechanisms: combination with biosorption affinity of the fungus and the enhanced intracellular accumulation by iron oxide nanoparticles. Possibly, the immobilization of *P. chrysosporium* with iron oxide nanoparticles and Ca-alginate endowed the adsorbents with higher adsorption capacities and good reusability, by the introduction of Fe—O groups and enhanced interior accumulation. Even after five cycles of adsorption–desorption, the adsorption ability was regained completely and the adsorption efficiency of Pb(II) was maintained above 90%. The desorption and reusability results indicated that the adsorbents were stable with good reusability. In conclusion, as-prepared adsorbents showed a promising prospect for application in heavy metal-containing wastewater treatment, with great adsorption capacity and even favorable stability.

Acknowledgments

The study was financially supported by the National Natural Science Foundation of China (51039001, 50808073, 50978088), the Hunan Key Scientific Research Project (2009FJ1010), the Hunan Provincial Natural Science Foundation of China (10JJ7005), the Environmental Protection Technology Research Program of Hunan (2007185), the New Century Excellent Talents in University (NCET-08-0181) and the Xiangjiang Water Environmental Pollution Control Projects Subjected to the National Key Science and Technology Project for Water Environmental Pollution Control (2009ZX0 7212-001-02 and 2009ZX0 7212-001-06).

References

[1] P. Xu, G.M. Zeng, D.L. Huang, C.L. Feng, S. Hu, M.H. Zhao, C. Lai, Z. Wei, C. Huang, G.X. Xie, Z.F. Liu, Use of iron oxide nanomaterials in wastewater treatment: a review, Sci. Total Environ. 424 (2012) 1–10.
[2] D.L. Huang, G.M. Zeng, C.L. Feng, S. Hu, M.-H. Zhao, C. Lai, Y. Zhang, X.Y. Jiang, H.L. Liu, Mycelial growth and solid-state fermentation of lignocellulosic waste by white-rot fungus *Phanerochaete chrysosporium* under lead stress, Chemosphere 81 (2010) 1091–1097.
[3] V.K. Gupta, A. Rastogi, A. Nayak, Adsorption studies on the removal of hexavalent chromium from aqueous solution using a low cost fertilizer industry waste material, J. Colloid Interface Sci. 342 (2010) 135–141.
[4] B. Southichak, K. Nakano, M. Nomura, N. Chiba, O. Nishimura, *Phragmites australis*: a novel biosorbent for the removal of heavy metals from aqueous solution, Water Res. 40 (2006) 2295–2302.
[5] V.K. Gupta, C. Jain, I. Ali, M. Sharma, V. Saini, Removal of cadmium and nickel from wastewater using bagasse fly ash – a sugar industry waste, Water Res. 37 (2003) 4038–4044.
[6] V.K. Gupta, D. Mohan, S. Sharma, Removal of lead from wastewater using bagasse fly ash-a sugar industry waste material, Sep. Sci. Technol. 33 (1998) 1331–1343.
[7] R. Naseem, S. Tahir, Removal of Pb(II) from aqueous/acidic solutions by using bentonite as an adsorbent, Water Res. 35 (2001) 3982–3986.
[8] V.K. Gupta, I. Ali, Removal of lead and chromium from wastewater using bagasse fly ash—a sugar industry waste, J. Colloid Interface Sci. 271 (2004) 321–328.
[9] V.K. Gupta, A. Rastogi, Biosorption of lead from aqueous solutions by green algae Spirogyra species: kinetics and equilibrium studies, J. Hazard. Mater. 152 (2008) 407–414.
[10] V.K. Gupta, M. Gupta, S. Sharma, Process development for the removal of lead and chromium from aqueous solutions using red mud – an aluminium industry waste, Water Res. 35 (2001) 1125–1134.
[11] Y.L. Lai, G. Annadurai, F.C. Huang, J.F. Lee, Biosorption of Zn(II) on the different Ca-alginate beads from aqueous solution, Bioresour. Technol. 99 (2008) 6480–6487.
[12] A.R. Mahdavian, M.A.S. Mirrahimi, Efficient separation of heavy metal cations by anchoring polyacrylic acid on superparamagnetic magnetite nanoparticles through surface modification, Chem. Eng. J. 159 (2010) 264–271.
[13] P. Yuan, M. Fan, D. Yang, H. He, D. Liu, A. Yuan, J.X. Zhu, T.H. Chen, Montmorillonite-supported magnetite nanoparticles for the removal of hexavalent chromium (Cr(VI)) from aqueous solutions, J. Hazard. Mater. 166 (2009) 821–829.
[14] M. Paljevac, M. Primožič, M. Habulin, Z. Novak, Ž. Knez, Hydrolysis of carboxymethyl cellulose catalyzed by cellulase immobilized on silica gels at low and high pressures, J. Supercrit. Fluid. 43 (2007) 74–80.
[15] S.H. Huang, M.H. Liao, D.H. Chen, Direct binding and characterization of lipase onto magnetic nanoparticles, Biotechnol. Prog. 19 (2003) 1095–1100.
[16] F. Sulek, M. Drofenik, M. Habulin, Z. Knez, Surface functionalization of silica-coated magnetic nanoparticles for covalent attachment of cholesterol oxidase, J. Magn. Magn. Mater. 322 (2010) 179–185.
[17] G.M. Zeng, D.L. Huang, G.H. Huang, T.J. Hu, X.Y. Jiang, C.L. Feng, Y.N. Chen, L. Tang, H.L. Liu, Composting of lead-contaminated solid waste with inocula of white-rot fungus, Bioresour. Technol. 98 (2007) 320–326.
[18] A. McHale, S. McHale, Microbial biosorption of metals: potential in the treatment of metal pollution, Biotechnol. Adv. 12 (1994) 647–652.
[19] K. Pakshirajan, T. Swaminathan, Biosorption of copper and cadmium in packed bed columns with live immobilized fungal biomass of *Phanerochaete chrysosporium*, Appl. Biochem. Biotechnol. 157 (2009) 159–173.
[20] U. Yetis, A. Dolek, F.B. Dilek, G. Ozceng, The removal of Pb(II) by *Phanerochaete chrysosporium*, Water Res. 34 (2000) 4090–4100.
[21] D.L. Huang, G.M. Zeng, X.Y. Jiang, C.L. Feng, H.Y. Yu, G.H. Huang, H.L. Liu, Bioremediation of Pb-contaminated soil by incubating with *Phanerochaete chrysosporium* and straw, J. Hazard. Mater. 134 (2006) 268–276.
[22] T.K. Kirk, S. Croan, M. Tien, Production of multiple ligninases by *Phanerochaete chrysosporium*: effect of selected growth conditions and use of a mutant strain, Enzyme Microb. Technol. 8 (1986) 27–32.
[23] T.K. Sen, S.P. Mahajan, K.C. Khilar, Adsorption of Cu^{2+} and Ni^{2+} on iron oxide and kaolin and its importance on Ni^{2+} transport in porous media, Colloids Surf. A 211 (2002) 91–102.
[24] Y.S. Ho, G. McKay, Pseudo-second order model for sorption processes, Process Biochem. 34 (1999) 451–465.
[25] J.P. Li, Q.Y. Lin, X.H. Zhang, Y. Yan, Kinetic parameters and mechanisms of the batch biosorption of Cr(VI) and Cr(III) onto *Leersia hexandra Swartz* biomass, J. Colloid Interface Sci. 333 (2009) 71–77.
[26] Y.S. Al-Degs, M.I. El-Barghouthi, A.A. Issa, M.A. Khraisheh, G.M. Walker, Sorption of Zn(II), Pb(II), and Co(II) using natural sorbents: equilibrium and kinetic studies, Water Res. 40 (2006) 2645–2658.
[27] D.L. Sparks, Kinetics of Soil Chemical Processes, Academic Press, New York, 1989.
[28] K. Varshney, A. Khan, U. Gupta, S. Maheshwari, Kinetics of adsorption of phosphamidon on antimony (V) phosphate cation exchanger: evaluation of the order of reaction and some physical parameters, Colloids Surf. A 113 (1996) 19–23.
[29] M. Iram, C. Guo, Y.P. Guan, A. Ishfaq, H.Z. Liu, Adsorption and magnetic removal of neutral red dye from aqueous solution using Fe_3O_4 hollow nanospheres, J. Hazard. Mater. 181 (2010) 1039–1050.
[30] V.K. Gupta, A. Rastogi, A. Nayak, Biosorption of nickel onto treated alga (*Oedogonium hatei*): application of isotherm and kinetic models, J. Colloid Interface Sci. 342 (2010) 533–539.
[31] L.V.A. Gurgel, L.F. Gil, Adsorption of Cu(II), Cd(II) and Pb(II) from aqueous single metal solutions by succinylated twice-mercerized sugarcane bagasse functionalized with triethylenetetramine, Water Res. 43 (2009) 4479–4488.
[32] N.K. Amin, Removal of reactive dye from aqueous solutions by adsorption onto activated carbons prepared from sugarcane bagasse pith, Desalination 223 (2008) 152–161.
[33] K. Fytianos, E. Voudrias, E. Kokkalis, Sorption–desorption behaviour of 2,4-dichlorophenol by marine sediments, Chemosphere 40 (2000) 3–6.
[34] F. Haghseresht, G.Q. Lu, Adsorption characteristics of phenolic compounds onto coal-reject-derived adsorbents, Energy Fuel 12 (1998) 1100–1107.
[35] Y.M. Hao, C. Man, Z.B. Hu, Effective removal of Cu(II) ions from aqueous solution by amino-functionalized magnetic nanoparticles, J. Hazard. Mater. 184 (2010) 392–399.
[36] I. Langmuir, The constitution and fundamental properties of solids and liquids. Part I. Solids, J. Am. Chem. Soc. 38 (1916) 2221–2295.
[37] K.R. Hall, L.C. Eagleton, A. Acrivos, T. Vermeulen, Pore-and solid-diffusion kinetics in fixed-bed adsorption under constant-pattern conditions, Ind. Eng. Chem. Fund. 5 (1966) 212–223.
[38] P. Kaewsarn, Biosorption of copper(II) from aqueous solutions by pre-treated biomass of marine algae *Padina* sp., Chemosphere 47 (2002) 1081–1085.
[39] Q. Li, S. Wu, G. Liu, X. Liao, X. Deng, D. Sun, Y. Hu, Y. Huang, Simultaneous biosorption of cadmium(II) and lead(II) ions by pretreated biomass of *Phanerochaete chrysosporium*, Sep. Purif. Technol. 34 (2004) 135–142.
[40] R. Say, A. Denizli, M. Yakup Arıca, Biosorption of cadmium(II), lead(II) and copper(II) with the filamentous fungus *Phanerochaete chrysosporium*, Bioresour. Technol. 76 (2001) 67–70.
[41] M. Iqbal, Biosorption of lead, copper and zinc ions on loofa sponge immobilized biomass of *Phanerochaete chrysosporium*, Miner. Eng. 17 (2004) 217–223.
[42] N.N. Nassar, Rapid removal and recovery of Pb(II) from wastewater by magnetic nanoadsorbents, J. Hazard. Mater. 184 (2010) 538–546.
[43] Y. Pang, G.M. Zeng, L. Tang, Y. Zhang, Y.Y. Liu, X.X. Lei, Z. Li, J.C. Zhang, Z.F. Liu, Y.Q. Xiong, Preparation and application of stability enhanced magnetic nanoparticles for rapid removal of Cr(VI), Chem. Eng. J. 175 (2011) 222–227.
[44] A. Bée, D. Talbot, S. Abramson, V. Dupuis, Magnetic alginate beads for Pb(II) ions removal from wastewater, J. Colloid Interface Sci. 362 (2011) 486–492.
[45] Z.Y. Yao, J.H. Qi, L.H. Wang, Equilibrium, kinetic and thermodynamic studies on the biosorption of Cu(II) onto chestnut shell, J. Hazard. Mater. 174 (2010) 137–143.
[46] Y. Seki, K. Yurdakoç, Adsorption of Promethazine hydrochloride with KSF Montmorillonite, Adsorption 12 (2006) 89–100.
[47] K.P. Yadava, B.S. Tyagi, V.N. Singh, Effect of temperature on the removal of lead(II) by adsorption on china clay and wollastonite, J. Chem. Technol. Biotechnol. 51 (1991) 47–60.

[48] S. Paul, D. Bera, P. Chattopadhyay, L. Ray, Biosorption of Pb(II) by *Bacillus cereus* M116 immobilized in calcium alginate gel, J. Hazard. Subst. Res. 5 (2006) 1–13.
[49] I. Tan, B. Hameed, Adsorption isotherms, kinetics, thermodynamics and desorption studies of basic dye on activated carbon derived from oil palm empty fruit bunch, J Appl. Sci. 10 (2010) 2565–2571.
[50] W.J. Weber, J.C. Morris, Kinetics of adsorption on carbon from solutions, J. Sanit. Eng. Div. Am. Soc Civ. Eng. 89 (1963) 31–60.
[51] V.K. Gupta, I. Ali, V.K. Saini, Defluoridation of wastewaters using waste carbon slurry, Water Res. 41 (2007) 3307–3316.
[52] R. Sheha, A. El-Zahhar, Synthesis of some ferromagnetic composite resins and their metal removal characteristics in aqueous solutions, J. Hazard. Mater. 150 (2008) 795–803.
[53] O. Keskinkan, M.Z.L. Goksu, A. Yuceer, M.F.C.F. Basibuyuk, Heavy metal adsorption characteristics of a submerged aquatic plant (*Myriophyllum spicatum*), Process Biochem. 39 (2003) 179–183.
[54] N. Lázaro, A.L. Sevilla, S. Morales, A.M. Marqués, Heavy metal biosorption by gellan gum gel beads, Water Res. 37 (2003) 2118–2126.
[55] S.S. Ahluwalia, D. Goyal, Microbial and plant derived biomass for removal of heavy metals from wastewater, Bioresour. Technol. 98 (2007) 2243–2257.
[56] D.L. Huang, G.M. Zeng, C.L. Feng, S. Hu, X.Y. Jiang, L. Tang, F.F. Su, Y. Zhang, W. Zeng, H.L. Liu, Degradation of lead-contaminated lignocellulosic waste by *Phanerochaete chrysosporium* and the reduction of lead toxicity, Environ. Sci. Technol. 42 (2008) 4946–4951.
[57] P. Persson, K. Axe, Adsorption of oxalate and malonate at the water–goethite interface: molecular surface speciation from IR spectroscopy, Geochim. Cosmochim. Acta 69 (2005) 541–552.
[58] L.S. Zhong, J.S. Hu, H.P. Liang, A.M. Cao, W.G. Song, L.J. Wan, Self-assembled 3D flowerlike iron oxide nanostructures and their application in water treatment, Adv. Mater. 18 (2006) 2426–2431.